RSC Advances

ROYAL SOCIETY OF CHEMISTRY

www.rsc.org/advances

RSC Advances

PAPER

A new microporous layer material to improve performance and durability of polymer electrolyte membrane fuel cells

Received 00th January 20xx,
Accepted 00th January 20xx

DOI: 10.1039/x0xx00000x

www.rsc.org/advances

Yongyi Jiang[a, b], Jinkai Hao[a, b], Ming Hou*[a], Hongjie Zhang[a, b], Xiaojin Li**[c], Zhigang Shao[a] and Baolian Yi[a]

Antimony doped tin oxide (ATO), a kind of semiconducting nanocrystalline, has excellent electrochemistry stability but poor electrical conductivity. Herein, ATO nanocomposites with carbon coatings are prepared via immersing ATO nano-material into dopamine solution, and then thermal treating to improve the electrical conductivity of ATO material. The morphology and microstructure of ATO@C/N nanocomposites are characterized using a scanning electron microscope and transmission electron microscopy. The GDLs with the MPL prepared by ATO@C/N nanocomposites are characterized by through-plane resistance test, mercury intrusion porosimetry and surface contact angle measurement. The above results show that ATO@C/N nanocomposites with a 2.16 nm thickness carbon coating enhance electrical conductivity of ATO nanocrystalline and exhibit higher electrochemical stability. Further, the performance of MEA fabricated with ATO@C/N as the cathode MPL is evaluated, with the maximum power density approaching to 1000 mW cm^{-2}, and a slight difference of cell performance is obersered compared to XC-72.

Introduction

The conclusions section should come in this section at the end of the article, before the acknowledgements. Durability is currently an increasingly important issue in proton exchange membrane fuel cells (PEMFCs).[1] In term of gas diffusion layer (GDL), one of major challenge derives from the corrosion of carbon material.[2-4] In general, GDL consists of a carbon paper or carbon cloth substrate and a microporous layer (MPL) composed of the mixture of carbon powder and polytetrafluoroethylene (PTFE). And its basic functions are the diffusion of reactant gas from flow channels to catalyst layer effectively, draining out liquid water from catalyst layer to flow channels, conducting electrons with low resistance.[5]

As a crucial part of GDL, MPL plays an important role in the improvement of the water management, thereby enhancing PEMFC performance and durability.[6] Carbon powder, for example Vulcan XC-72, is commonly used as commercial MPL material. However, the greatest trouble of carbon is hard to keep electrochemical stability under high-oxidization acidic circumstances although it can ensure good fuel cell performance. There have been a few studies on GDL, such as effects on the treatment with different amount PTFE,[7-9] degradation mechanism of carbon,[10-12] hydrophilic and hydrophobic treatment of MPL.[6, 13] However, few involve the alternative of carbon powder or pay attention to new MPL material. Therefore, it is meaningful to introduce other new kind of material, replacing the carbon powder. Antimony doped tin oxide (ATO) is a good alternative for the MPL material because of its physical and chemical properties: it is a typical n-type semiconducting material with excellent stability and its electrical conductivity is affected by the molar content of antimony.[14, 15] ATO is stable in acidic media and has much higher corrosion resistance compared with the carbon material,[16] which makes it widely used as an electronic conducting coatings, gas sensors, solar battery transparent electrodes.[17] However, the relative lower conductivity is always its major problem compared with Vulcan XC-72.

To apply a conductive carbon coating onto the ATO's surface is an effective approach to the improvement of electronic conductivity. It has been noted that the carbon coating can enhance the electrochemical performance of the nanocomposites.[18-20] However, one key issue must be considered: the carbon coating should be uniform and continuous to provide rapid and continuous electronic transport.[18] To fully achieve this approach, dopamine, a kind of biomolecule that has a strong and versatile adhesion capability, is commonly used as a coating agent and carbon precursor. This function of dopamine lies in its chemical structure that incorporates many functional groups such as catechol and amine. And it can easily self-polymerize to form

[a] [a] Fuel Cell System and Engineering Laboratory, Dalian Institute of Chemical Physics, Chinese Academy of Sciences, 457 Zhongshan Road, Dalian 116023, China.
[b] [b] University of Chinese Academy of Sciences, Beijing 100039, China.
[c] [c] Qingdao Institute of Bioenergy and Bioprocess Technology, Chinese Academy of Sciences, 189 Songling Road, Qingdao 266101,China.
* Co-corresponding author. Tel.: +86-411-84379051; Fax: +86-411-84379185;E-mail addresses: houming@dicp.ac.cn (M. Hou)
** Corresponding author. Tel.: +86-532-80662649; Fax: +86-532-80662778; E-mail address: lixj@qibebt.ac.cn (X. Li)

PAPER

polydopamine coating on a types of substrate, including inorganic and organic

Scheme 1. Schematic illustration of the fabrication of ATO@C/N nanocomposites

surface, at alkaline pH values under oxygen atmosphere.[21, 22] One valuable feature of polydopamine is that the thickness of coating layer can be controlled through varying the initial concentration of dopamine or the polymerization time.[23, 24] Therefore, using dopamine as a coating agent and carbon precursor has a significant advantage in tuning the compositions and properties of the coating layer, which is important for material design and optimization.

In our work, ATO is ~~creatively~~ applied to MPL and converted into ATO@C/N nanocomposite after the immersing into dopamine solution and thermal treatment. This new cathode MPL prepared with ATO@C/N nanocomposites had better electrochemical stability but lower electrical conductivity and slightly poorer cell performance compared with XC-72 MPL. Nevertheless, its maximum power density approached 1000 mW cm^{-2} at 2300 mA cm^{-2}.

Experimental

Materials

The main text of the article should appear here with headings as appropriate. Dopamine hydrochloride with MW of 189.64, purity 98%, was obtained from Aladdin. ATO nanoparticle (purity >99.97%, Sb_2O_5:SnO_2 10:90 wt.%, particle size 7-15 nm, BET surface area 65-80 m^2 g^{-1}, specific volume resistance <10 Ω·cm) was purchased from NERCN Co., China.

Preparation of ATO@C/N particles

Typically, 600 mg ATO were dispersed into 50 mL Tris-buffer (pH 8.5) to form a suspension under magnetic stirring for 30 min. Then added 100 mg dopamine into the above mixtures under moderate stirring for 24 h. After that, centrifugalized the sample 4 times at the rotational speed 8000 rpm and 5 minutes per time. Subsequently, the above sample was dried under vacuum with 60 °C for 24 hours. Then grinded the above powders and obtained ATO particles with definite thickness of polydopamine coating. Finally, heated the powders in quartz tube under Ar atmosphere at heating-up speed of 5 °C min^{-1} with 160 °C for 1 h, 500 °C for 4 h based on the procedure presented in Ref.[18] After natural cooling, ATO powders with N-doped carbon coating were obtained and named as ATO@C/N.

Preparation of the cathode GDL

GDL (Sunrise Power Co., Ltd., China.) consists of a substrate and a MPL and the substrate commonly uses commercial carbon paper (Toray) treated with PTFE to add hydrophobic property. The MPL slurry is prepared by mixing 64 mg Vulcan XC-72 (Cabot China Ltd.) into 640 mg 5 wt% PTFE. To prepare the cathode GDL, the MPL slurry should be coated onto one side of the as-treated carbon paper by rolling with a glass rod. Then take it into an oven with 80 °C and sinter it at 240 °C for 30 min and 350 °C for 90 min under nitrogen ambience. The new cathode GDL should take 320 mg ATO@C/N nanocomposites or ATO particles into 640 mg 5 wt% PTFE and sinter it in the same conditions. Pressed disc method was adopted to keep the same volume fraction of XC-72 and ATO on GDL material in the preparation process.

Material characterization

The morphology and microstructure of ATO@C/N nanocomposites were characterized using a scanning electron microscope (SEM, JSM 6360-LV) and transmission electron microscopy (TEM, JEOL JEM-2000EX) operating at 120 kV. The element content and distribution onto nanocomposites were characterized by Energy dispersive X-ray spectroscopy (EDS) at SEM. To compare the pore size distribution and porosity for different GDLs the mercury intrusion porosimetry (PoreMasterGT 60) was adopted. The pore size distribution curve was determined according to the volume of mercury penetrating the pores versus the applied pressure. Besides, surface contact angles of GDLs were also measured using the Drop Shape Analyzer (DSA 100).

The through-plane resistance of cathode GDL was measured using mechanical device under compression. The untested sample (1×2 cm^2) was placed between two coated gold bullions applied to a 5 A electrical current. The tested pressure was applied from 1 to10 kg cm^{-2} with 1 kg increment under the rate of 0.1 mm min^{-1}. Once the tested pressure reached the set value,

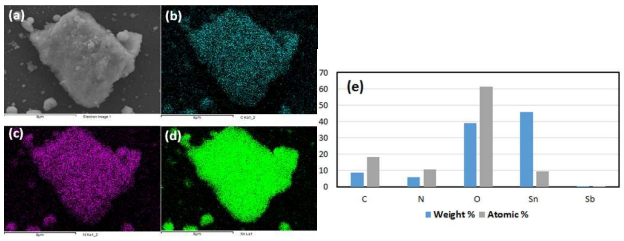

Fig. 1 (a) SEM image of ATO@C/N; EDS element maps of (b) C element, (c) N element, (d) Sn element; and (e) Element content distribution chart of ATO@C/N nanocomposites.

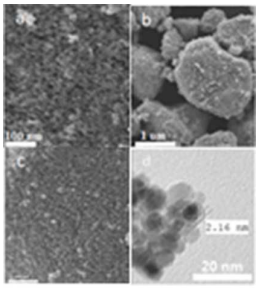

Fig. 2 a) SEM image of ATO; b), c) SEM and d) TEM images of ATO@C/N.

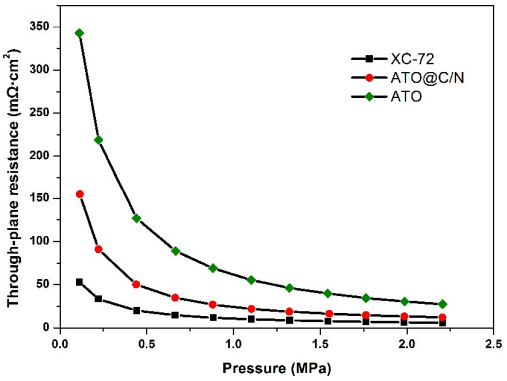

Fig. 3 Through-plane resistance of different GDL materials.

the relevant voltage value was recorded. The through-plane resistance was calculated by equation (1) [25].

$$R=US/2I \quad (1)$$

Where *R* was the through-plane resistance, *U* was the voltage, *S* was the area of tested sample and *I* was the current.

Electrochemical characterization

The electrochemical measurements of ATO@C/N sample were performed using CHI730 electrochemical station by the conventional three-electrode method, which consisted of as-prepared samples (working electrode), saturated calomel electrode (SCE, reference electrode) and a Pt foil (counter electrode). These tests were conducted in 0.5 M H_2SO_4 solution saturated with high purity N_2 and all the potentials were given versus the normal hydrogen electrode (NHE). The chronoamperometric testing was profiled 2 hours to oxidize MPL materials at a constant potential of 1.2 V. Moreover, cyclic voltammetry (CV) measurements were carried out before and after oxidization with a scan rate of 50 mV s^{-1} and the cycling potential from -0.241 and 0.959 V.[10] The carbon powder (XC-72) was also prepared the working electrode and suffered the same testing to judge the anti-corrosion ability of different MPL materials.

Furthermore, electrochemical stability of cathode GDL materials were tested via the three-electrode method in a homemade testing setup by BiStat potentiostat. The as-prepared GDL (1×2 cm^2) was used as the working electrode. The graphite plate and saturated calomel electrode were employed as the counter electrode and reference electrode, respectively. To simulate the operating conditions of fuel cell, the testing were performed 24 h in 0.5 M H_2SO_4 solution saturated with high purity N_2 at 70 °C.

Single-cell assembly and performance tests

The new cathode GDL prepared with ATO@C/N nanocomposites was assembled for a single fuel cell. Catalyst coated membrane (CCM), consisted of a Nafion 212 membrane and the Pt/C catalyst with the Pt loading of 0.2 and 0.4 mg cm^{-2} at anode and cathode, was sandwiched with new cathode GDL and the normal anode GDL through hot-pressing method at 140 °C for 2 min. The utilizable areas of fuel cell was 5.0 cm^2. The fuel cell performance was measured through a fuel cell impedance meter (KFM2030, Kikusui). During the test, the cell temperature was 65 °C and the humidification temperature was 65 °C for H_2/O_2. The flow rate of H_2/O_2 was 50/100 mL min^{-1} at 0.05 MPa. For comparison, other fuel cells were prepared with commercial GDL and the same CCM and tested in the same conditions.

Results and discussion

Preparation samples

Scheme 1 illustrates the fabrication process of ATO@C/N nanoparticles. Initially, ATO nanoparticles were coated with polydopamine through immersing ATO into a dopamine buffer solution (pH=8.5). During the immersion, the polymerization of dopamine monomers occurred via a pH-induced oxidation, coupled with a color change from light blue to dark brown after 24 h. Afterwards, the ATO@polydopamine composites were annealed at 500 °C for 4 h to convert ATO@C/N.

Physical characterization

The energy-dispersive X-ray spectroscopy (EDS) elemental mapping of the ATO@C/N nanocomposites (Fig. 1a) shows the existence of N element, demonstrating that polydopamine has been transformed into N-droped carbon coating on the ATO surface after pyrolysis. In addition, the signals of C, N and Sn on the EDS maps confirm the uniform and continuous distribution of the above elements throughout the nanocomposites, which can provide rapid and continuous electronic transport and contribute to the increasing electric conductivity of ATO material. Fig. 1b shows the element content of ATO@C/N nanocomposites. The nitrogen content on the surface of ATO@C/N was calculated to be 5.94 wt. % through the EDS and a bit lower than carbon content (8.85 wt.%). which fited in with the molecular structure of dopamine.

The morphology of the as-prepared ATO@C/N is examined by scanning electron microscopy (SEM) and transmission electron microscopy (TEM). Fig. 2b and 2c show the SEM images of ATO@C/N, which presents the sense of satiation after the ATO particles coated with carbon and nitrogen compared with pure ATO of Fig. 2a. In addition, Fig. 2d reveals TEM image of ATO@C/N and the thickness of the C/N coating was approximately 2 nm.

Through-plane resistance

The through-plane resistance of GDL materials has a significant effect on the contact resistance of catalyst layer and affects

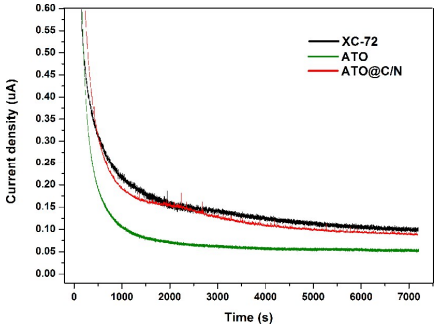

PAPER

Fig. 4 Chronoamperometric curves for XC-72, ATO and ATO@C/N samples measured at 1.2 V vs NHE in nitrogen-purged 0.5 M H2SO4.

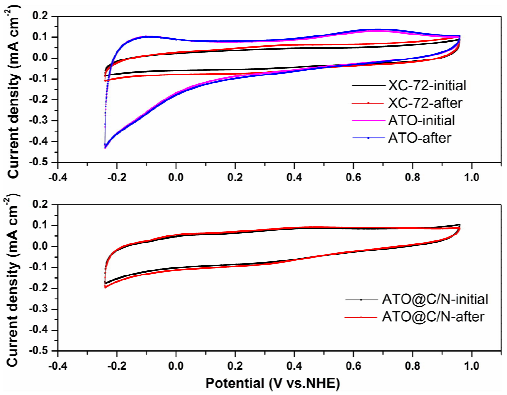

Fig. 5 CV curvres of XC-72, ATO and ATO@C/N samples under potential cycling between -0.241 and 0.959 V oxidation in 0.5 M H_2SO_4 electrolyte, with a scan rate of 50 mV s^{-1}.

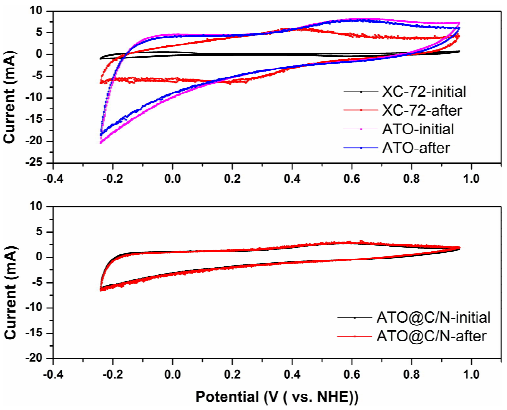

Fig. 6 CV curvres of GDL prepared by XC-72, ATO and ATO@C/N samples at 70 °C under potential cycling between -0.241 and 0.959 V oxidation in 0.5 M H_2SO_4 electrolyte, with a scan rate of 50 mV s^{-1}.

the output performance of fuel cell finally [26]. Fig. 3 compares the through-plane resistance of different GDL materials. The GDL prepared by XC-72 has the least through-plane resistance and the highest value of ATO material's. The ATO@C/N shows a lower through-plane resistance than pristine ATO, but higher than XC-72 powder in particular under higher pressure. Consequently, ATO particle with coating treatment indeed improved its electrical conductivity.

Electrochemical studies

To evaluate the electrochemistry stability of XC-72, ATO and ATO@C/N samples, the potential value of Potentiostatic oxidation is set 1.2 V (vs NHE). Because the hydrolysis reaction of water does not happen under this potential value, the main reaction occurred is the corrosion of carbon material [2, 12]. And the corrosion current is increasing with the intensification of corrosion reaction. Fig. 4 shows the chronoamperometric curves of XC-72, ATO and ATO@C/N samples under constant potential (1.2V vs NHE) for 2 h. As seen, the corrosion current of ATO@C/N was approximately 0.084 μA, which was 16.8% less than that of XC-72 (0.101 μA) and 36.8% more than that of ATO (0.052 μA). The results indicated that ATO@C/N nanoparticle after coating treatment still had higher electrochemistry stability than XC-72 although it decreased compared with pristine ATO.

The durability of the above materials is also evaluated by CV measurements test before and after oxidation treatment at the cycling potential from -0.24 and 0.96 V (vs. NHE). In Fig. 5, there was a significant disaccord between XC-72 CV curves and ATO, ATO@C/N curves. It should be note that the CV curve of ATO@C/N had the least change, which indicated ATO@C/N nanocomposite had more stability. It was to say that ATO@C/N nanocomposite performed better than XC-72 in terms of the anti-corrosion ability.

To further evaluate the anti-corrosion stability of MPL materials, GDLs are tested by potentiostat under the simulated fuel cell environments. Fig. 6 shows the CV curves of different GDLs at 70 °C. Comparing the CV diagrams before and after oxidation, it could be seen that the GDL with ATO@C/N not only had higher ability than XC-72 GDL to resist corrosion under high-oxidization acidic circumstances, but performed better than ATO GDL. Other researchers [10] illustrated that the stability decrease of GDL prepared by XC-72 derived from the oxidization of carbon surface, which could be confirmed by the peak current on the CV curves. The peak current of 0.4 V (vs SCE) corresponds with the quinone-hydroquinone redox couple which is an oxygen-containing substances produced from the oxidization process of carbon. Based on the above electrochemical tests, a comprehensive results can be drawn that the ATO@C/N nanocomposites, accompanying with thinner carbon coating, keep back the stability of ATO materials well and avoid the prone to corrosion owing to thicker carbon coating.

Mercury intrusion porosimetry and contact angle measurement

Besides, mercury intrusion porosimetry is carried out to evaluate the pore size distribution of different GDLs. Fig. 7 is the pore size distribution diagrams of different GDLs prepared with XC-72 and ATO@C/N, which can be seen clearly that both curves have similar change of pore size, especially in pore size range displaying the little difference between above GDLs. The mercury intrusion porosimetry also provides porosity and specific pore volume. In table 1, GDL with ATO@C/N nanocomposites had lower porosity and specific pore volume but higher mean pore diameter compared with XC-72 GDL, which could be presumed that the micropores used to transmit water in the MPL had a lower proportion. The surface contact angle images as a thumbnail is inserted in the Fig. 7.

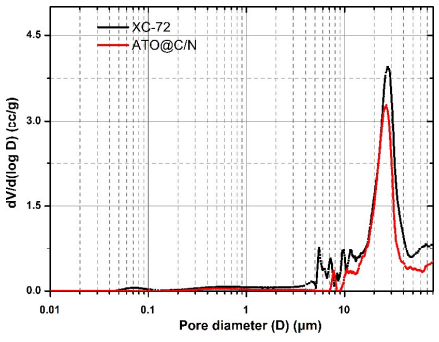

Fig. 7 Pore size distribution curves and surface contact angle images of GDLs prepared with XC-72 and ATO@C/N.

Table 1 Mean Pore Diameter, specific Pore Volume and porosity of GDLs prepared with XC-72 and ATO@C/N.

	Mean Pore Diameter (μm)	Specific Pore Volume (mL/g)	Porosity* (%)
XC-72	17.37	7.08	20.17
ATO@C/N	60.34	6.83	12.24

* Based on the pores with a range of 0 ~ 100 micron.

It was obvious that ATO@C/N GDL has a lower contact angle and a weak hydrophobicity relative to XC-72 GDL.

Single-cell performance tests

Fig. 8 displays the single-cell performance of cathode MPL with ATO, ATO@C/N and the commercial XC-72 powder. As seen, this new cathode MPL prepared with ATO@C/N nanocomposites showed a close performance except at high current density compared with XC-72 cathode MPL. In addition, it performed a significantly improved performance compared to the cell with ATO MPL, and its maximum power density approached 1000 mW cm^{-2} at 2300 mA cm^{-2}, which demonstrated the enhanced conductivity of ATO@C/N material indeed improved the cell performance. However, under a higher current density, the slightly poor performance of ATO@C/N GDL compared to XC-72 GDL on the one hand could be ascribed to its electrical conductivity, and on the other hand was an imperfect water management which was confirmed by the previous mercury intrusion porosimetry. The more hydrophobic the micropore is, the more easily water is discharged.[27] GDL prepared by ATO@C/N with a lower proportion of micropore would hinder water transportation, and its poor hydrophobicity would even cause "flooded". Although this new cathode MPL material hasn't exceeded the commercial XC-72 yet, concerning the good electrochemical durability and compromise conductivity of ATO@C/N nanocomposites, applied it in PEMFC field is still promising. Future work will be focused on i) exploration of fuel cell performances under low relative humidity, particularly high temperature PEMFC conditions [28] and ii) improving the hydrophobicity of ATO material on the premise of good electrical conductivity.

Conclusions

In summary, ATO nanocomposites with N-doped carbon coating were synthesized using dopamine as the coating agent and carbon precursor. The new cathode MPL prepared with ATO@C/N exhibited better electrochemical stability than XC-72 MPL and higher electrical conductivity than ATO MPL. However, ATO@C/N MPL had slightly poor cell performance compared to XC-72 MPL in view of its poor hydrophobicity and lower micropore percentage. Nevertheless, the results still demonstrate that ATO material is a promising alternative of commercial Vulcan XC-72 for cathode MPL through a proper treatment.

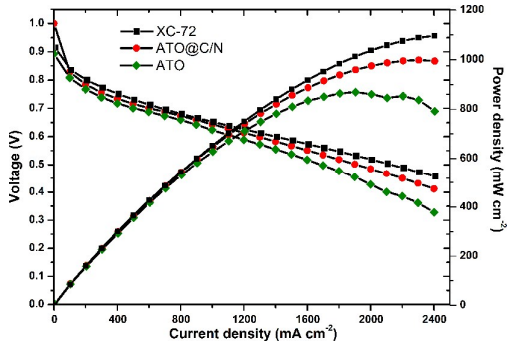

Fig. 8 Polarization and power density curves of fuel cells with different cathode MPLs. Measurements were taken at 65 °C with fully humidified reactants (flow rate was 50/100 mL min^{-1} for H_2/O_2) and at 0.05 MPa.

Acknowledgements

This work was financially supported by the National Key Basic Research Program of China (973 Program, No. 2012CB215505) and the National Natural Science Foundation of China (No. 61433013)

References

1. J. Xie, D. L. Wood, D. M. Wayne, T. A. Zawodzinski, P. Atanassov and R. L. Borup, *Journal of the Electrochemical Society*, 2005, **152**, A104-A113.
2. L. M. Roen, C. H. Paik and T. D. Jarvic, *Electrochemical and Solid State Letters*, 2004, **7**, A19-A22.
3. B. Merzougui and S. Swathirajan, *Journal of the Electrochemical Society*, 2006, **153**, A2220-A2226.
4. H.-S. Oh, J.-H. Lee and H. Kim, *International Journal of Hydrogen Energy*, 2012, **37**, 10844-10849.
5. L. Cindrella, A. M. Kannan, J. F. Lin, K. Saminathan, Y. Ho, C. W. Lin and J. Wertz, *Journal of Power Sources*, 2009, **194**, 146-160.
6. T. Kitahara, H. Nakajima and K. Mori, *Journal of Power Sources*, 2012, **199**, 29-36.
7. S. Kim, B.-H. Jeong, B. K. Hong and T.-S. Kim, *Journal of Power Sources*, 2014, **270**, 342-348.
8. R. J. F. Kumar, V. Radhakrishnan and P. Haridoss, *International Journal of Hydrogen Energy*, 2012, **37**, 10830-10835.
9. G. G. Park, Y. J. Sohn, T. H. Yang, Y. G. Yoon, W. Y. Lee and C. S. Kim, *Journal of Power Sources*, 2004, **131**, 182-187.
10. S. Yu, X. Li, S. Liu, J. Hao, Z. Shao and B. Yi, *Rsc Advances*, 2014, **4**, 3852-3856.
11. T. Ha, J. Cho, J. Park, K. Min, H.-S. Kim, E. Lee and J.-Y. Jyoung, *International Journal of Hydrogen Energy*, 2011, **36**, 12436-12443.
12. G. Chen, H. Zhang, H. Ma and H. Zhong, *International Journal of Hydrogen Energy*, 2009, **34**, 8185-8192.
13. T. Kitahara, H. Nakajima, M. Inamoto and M. Morishita, *Journal of Power Sources*, 2013, **234**, 129-138.
14. W. Qu, Z. Wang, X. Sui and D. Gu, *International Journal of Hydrogen Energy*, 2014, **39**, 5678-5688.
15. M. Yin, J. Xu, Q. Li, J. O. Jensen, Y. Huang, L. N. Cleemann, N. J. Bjerrum and W. Xing, *Applied Catalysis B-Environmental*, 2014, **144**, 112-120.
16. K.-S. Lee, I.-S. Park, Y.-H. Cho, D.-S. Jung, N. Jung, H.-Y. Park and Y.-E. Sung, *Journal of Catalysis*, 2008, **258**, 143-152.
17. V. K. Puthiyapura, M. Mamlouk, S. Pasupathi, B. G. Pollet and K. Scott, *Journal of Power Sources*, 2014, **269**, 451-460.
18. C. Lei, F. Han, D. Li, W.-C. Li, Q. Sun, X.-Q. Zhang and A.-H. Lu, *Nanoscale*, 2013, **5**, 1168-1175.
19. Y. Ma, G. Ji, B. Ding and J. Y. Lee, *Journal of Materials Chemistry A*, 2013, **1**, 13625-13631.
20. Y. Ma, C. Zhang, G. Ji and J. Y. Lee, *Journal of Materials Chemistry*, 2012, **22**, 7845-7850.
21. F. Bernsmann, V. Ball, F. Addiego, A. Ponche, M. Michel, J. J. de Almeida Gracio, V. Toniazzo and D. Ruch, *Langmuir*, 2011, **27**, 2819-2825.
22. Y. Liu, K. Ai and L. Lu, *Chemical Reviews*, 2014, **114**, 5057-5115.
23. B. P. Lee, C. Y. Chao, F. N. Nunalee, E. Motan, K. R. Shull and P. B. Messersmith, *Macromolecules*, 2006, **39**, 1740-1748.
24. A. A. Ooka and R. L. Garrell, *Biopolymers*, 2000, **57**, 92-102.
25. J. Hao, S. Yu, Y. Jiang, X. Li, Z. Shao and B. Yi, *Journal of Electroanalytical Chemistry*, 2015, **756**, 201-206.

26. T. J. Mason, J. Millichamp, T. P. Neville, A. El-kharouf, B. G. Pollet and D. J. L. Brett, *Journal of Power Sources*, 2012, **219**, 52-59.
27. X. Wang, H. Zhang, J. Zhang, H. Xu, X. Zhu, J. Chen and B. Yi, *Journal of Power Sources*, 2006, **162**, 474-479.
28. J. Luo, A. H. Jensen, N. R. Brooks, J. Sniekers, M. Knipper, D. Aili, Q. Li, B. Vanroy, M. Wuebbenhorst, F. Yan, L. Van Meervelt, Z. Shao, J. Fang, Z.-H. Luo, D. E. De Vos, K. Binnemans and J. Fransaer, *Energy & Environmental Science*, 2015, **8**, 1276-1291.